ELSEVIER

Combustion and Flame 135 (2003) 87–96

Combustion and Flame

The extinction limits of a hydrogen counterflow diffusion flame above liquid oxygen

Matthew Juniper, Nasser Darabiha, Sébastien Candel*

Laboratoire EM2C, CNRS, Ecole Centrale Paris, 92295, Châtenay-Malabry (FRANCE)

Abstract

A counterflow diffusion flame between gaseous hydrogen and liquid oxygen (LOx) is studied numerically at 1 and 2 bar pressures. Conditions at the liquid interface are modelled using the Clausius-Clapeyron relation and the species profiles are evaluated with a one-dimensional numerical code. Complex chemistry and multicomponent transport are employed. Thermodynamic and transport properties are taken from Chemkin and the corresponding Transport packages. Typical species and temperature profiles are presented. The extinction strain rate is evaluated as a function of the inlet hydrogen temperature. This varies from 1.2×10^5 s^{-1} at a hydrogen temperature of 20K to 6.0×10^5 s^{-1} at a temperature of 310K, indicating that hydrogen/LOx flames are extremely resistant to strain rate. The effect of the temperature gradient on the liquid side of the interface is examined and found to be negligible. When applied to one aspect of the flame-holding in cryogenic rocket motors, these results may be used to infer that extinction by strain rate is improbable in the injector near-field, even for very low hydrogen stream temperatures.

Keywords: Strained flames; Extinction; Cryogenic combustion

1. Introduction

The successful launch of a rocket requires steady thrust from the engine with a well controlled ignition transient and a minimum level of vibration. High performance is particularly important in order to put an economically-viable mass into orbit. This is obtained by using cryogenic propellants, despite the considerable practical difficulties associated with these substances. In many engines, gaseous hydrogen and liquid oxygen are injected coaxially through a large number of injectors, that are mounted on the back wall of the combustion chamber. The flame stabilizes in the wake of the oxygen injector lip and develops in the near vicinity of the oxygen stream. The experimental image shown in Fig. 1 indicates that the flame edge is very close to the oxygen injector lip and that the flame spreads in the near vicinity of the LOx stream. Figure 2 gives a schematic representation of the flame in the near field and indicates that the stabilization takes place in an initially laminar region near the lip and close to the oxygen stream. This configuration has been investigated in numerical [1], and experimental studies [2–4]. Under normal operating conditions the flame is stable and it spreads as a highly turbulent brush. Below a critical hydrogen feed temperature, oscillations occur at frequencies corresponding to the chamber's acoustic modes [5]. Temperature seems to control the onset of these oscillations which suggests that the flame could lift off the oxygen injector making it more sensitive to acoustic coupling. With appropriate feedback this would lead to the observed oscillations. Given the power generated by the motor, combustion oscillations can lead to payload damage or even cata-

* Corresponding author. Tel.: +33-1-41-13-10-83; fax: +33-1-47-02-80-35.

E-mail address: candel@em2c.ecp.fr (S. Candel).

0010-2180/03/$ – see front matter
doi:10.1016/S0010-2180(03)00000-0

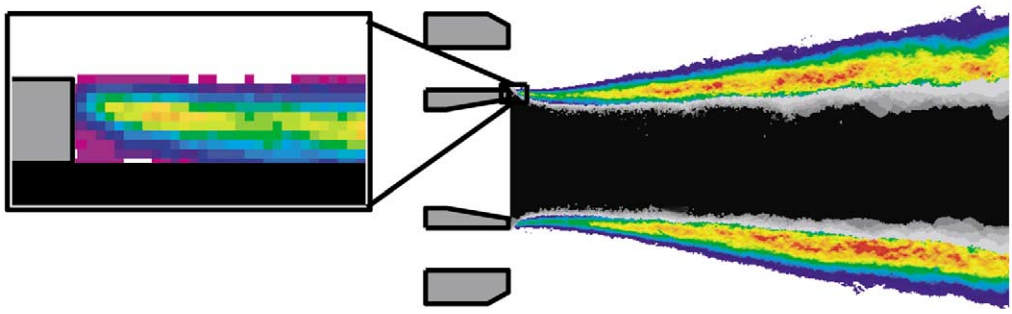

Fig. 1. Image of the flame formed between liquid oxygen and gaseous hydrogen in a typical cryogenic fuel injector. A slice of the average emission intensity is shown in color. The average oxygen jet position is shown in grayscale. The near-injector region is expanded on the left.

strophic failure of the rocket. In this article, one mechanism of flame lift-off is studied.

Once it is established, the flame runs approximately parallel to the hydrogen flow in the near-injector region (Fig. 1). Although strain parallel to the flame will not affect it, a turbulent eddy could impinge directly onto the surface, pinching the flame between the cold condensed oxygen and a fast perpendicular flow of cold hydrogen. It is known that diffusion flames formed between two low temperature reactant streams extinguish relatively easily, since heat loss takes place on both sides of the flame. This is unlike premixed flames which are backed by hot gases. The proximity of the condensed oxygen might significantly lower the strain rate at which this occurs. Once a hole has been punched in the diffusion flame an edge flame forms. The consequences of this have already been studied in a different context [6]. This edge flame does not then close up, even if the strain rate is immediately reduced. This means that holes will tend to grow if the extinction strain rate is exceeded for even a short time, and the flame will blow off, perhaps leaving a small pilot flame just behind the oxygen tube lip.

The most severe scenario occurs when an eddy arrives perpendicular to the surface. This can be modelled as a counterflow flame above a condensed fuel, as shown in Fig. 3. The flat flame formed in this configuration is submitted to an external strain rate. Extinction conditions may be studied by progressively increasing the strain rate until the temperature and reaction rate suddenly drop to vanishingly small values. Under a standard transformation this configuration can be reduced to a one-dimensional problem. While gaseous strained flames have been studied extensively, the case of a gaseous stream impinging on a liquid surface is less well documented. It is first considered in an asymptotic analysis with finite rate chemistry in the thermodiffusive limit [7]. It is demonstrated in this reference that extinction occurs

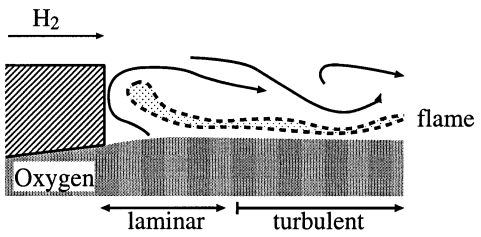

Fig. 2. Diagram of the stabilization mechanism in the wake of the lip of the liquid oxygen injector. The flow is laminar in the hot zone just behind the lip. Conditions become turbulent within a short distance. The flame can be pinched between the cold hydrogen flow and the liquid oxygen surface, which must evaporate in order to supply the flame. These harsh conditions could lead to local extinction and blow-off.

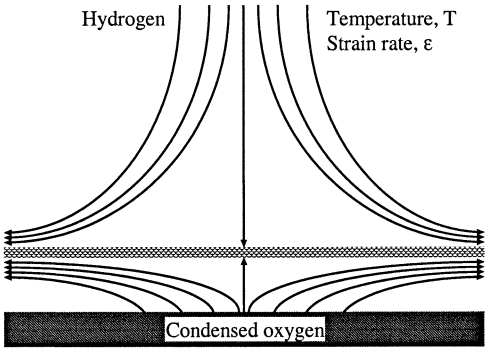

Fig. 3. Configuration of the model problem in the (x,z) plane (x axis horizontal). A counterflow hydrogen diffusion flame is situated above a pool of condensed oxygen. This can be reduced to a one-dimensional problem from which the extinction strain rate can be calculated as a function of the operating conditions.

when a Damköhler number based on the flow time divided by the chemical time is reduced below a critical level. This Damköhler number is proportional to B/ϵ_s, where B is the Arrhenius pre-exponential factor, and ϵ_s the strain rate. Vaporization processes seem not to be influential, a fact which is confirmed later in this article. The asymptotic analysis by Hamins [8] provides a way of calculating the extinction Damköhler number but comparison with experiments shows that this method is not always accurate. The problem is envisaged [9] in the infinitely fast chemistry limit to evaluate the vaporization rate and the flame position. This study also shows that when the Lewis number is unity, the counterflow flame is stable with respect to small fluctuations in strain rate and thermodynamic parameters at the liquid surface. It is assumed here that this remains true in the general case. With this assumption it is sufficient to calculate the extinction strain rate in steady flow. This assumption is backed up by the fact that the flame can survive at even higher strain rates when it is unsteady, but not pierced [10]. The situation is also considered in experiments [11,12], although neither reference tests the influence of the liquid properties. Other investigations of the structure of liquid oxygen/hydrogen flames have been carried out [13,14] but focus on the single droplet spherical flame problem or on the counterflow spray configuration.

In summary, this paper examines a counterflow diffusion flame between gaseous hydrogen and a layer of liquid oxygen. A one-dimensional model with complex chemistry and multi-component transport is used to evaluate stationary solutions. The strain rate varies from low values of 100 s^{-1} to the extinction strain rate and the hydrogen stream temperature is assigned values between 20 K and 310 K. In this way the extinction limit strain rate is evaluated as a function of the hydrogen temperature. The temperature gradient on the liquid side is also changed. As well as providing practical information on extinction limits, the results presented here confirm some previously cited analyses and highlight some aspects which could be examined further in future work.

2. Boundary conditions and governing equations

The formulation of the governing equations including complex chemistry and detailed transport is straightforward. However, the boundary conditions at the condensed phase require some care and this is discussed first.

2.1. Formulation of subcritical vs. supercritical problems

To one side of the flame is pure gaseous hydrogen at constant temperature. This is an easy boundary condition to model. The operating pressure of rocket engines is around 100 bar, above the critical pressure of both fluids. However, during the ignition process when oscillations have been observed, the pressure is below oxygen's critical pressure. The flame lies close to this condensed oxygen. Therefore, particular attention must be paid to the boundary condition on this side.

Below the critical pressure of pure oxygen, ($P_c \approx 5.0$ MPa) a liquid/vapour interface will always exist. Conditions at this interface are expressed in terms of the Clausius-Clapeyron equation (Eq. 1) which relates the saturation pressure, p_s to the surface temperature, T_s:

$$p_s(T_s) = p_0 \exp\left(\frac{\Delta h_v}{r_g} \left[\frac{1}{T_0} - \frac{1}{T_s} \right] \right) \tag{1}$$

Here the point (p_0, T_0) lies on the liquid/vapour phase equilibrium line, Δh_v is the latent heat of vaporization and r_g is the gas constant. From this relation, the composition at the surface can be evaluated. The heat flux is also related to the mass flux, $\dot{m}$, at the liquid interface by Eq. 2.

$$\lambda_v \frac{dT}{dx}\Big|_v = \dot{m} \Delta h_v + \lambda_l \frac{dT}{dx}\Big|_l \tag{2}$$

where λ_v and λ_l denote the thermal conductivities on the vapour and the liquid sides respectively.

The liquid and gas phases can be simulated separately, with jump conditions at the interface linking the two domains. This permits the use of an optimized equation of state and multispecies transport formulations in each phase. At the expense of some accuracy, simulation of the liquid phase can be replaced by the assumption that it is pure oxygen. Thus, only the gaseous phase needs to be simulated. It can be checked *a posteriori* that the concentrations of other species at the interface are quite small.

Above the critical pressure of pure oxygen ($p > P_c$), it cannot be assumed *a priori* that an interface will exist and it is not possible in this case to split the simulation up into liquid and vapour phases. Subcritical conditions are therefore assumed in this analysis.

2.2. Governing equations

The planar (x,z) counterflow flame (Fig. 3) is reduced to a one-dimensional problem along the z axis by assuming that the flow-field is of the form:

$$u = U(z)\,x, \; \rho v = V(z) \tag{3}$$

where u is the velocity in the x-direction, parallel to the liquid surface and v is the velocity in the z-direction, perpendicular to the surface. The transverse pressure gradient, $J \equiv -(1/x)\partial p/\partial x$, is unknown but is assumed to be constant in the z-direction. In the stationary case the balance equations for mass, momentum, species and energy take the following form:

$$\rho U + \frac{\partial(\rho v)}{\partial z} = 0 \tag{4}$$

$$\rho U^2 + \rho v \frac{\partial U}{\partial z} - J - \frac{\partial}{\partial z}\left(\mu \frac{\partial U}{\partial z}\right) = 0 \tag{5}$$

$$\rho v \frac{\partial Y_k}{\partial z} + \frac{\partial}{\partial z}(\rho Y_k V_k) - \omega_k W_k = 0,\ k = 1, \ldots, \mathrm{N} \tag{6}$$

$$\rho v c_p \frac{\partial T}{\partial z} - \frac{\partial}{\partial z}\left(\lambda \frac{\partial T}{\partial z}\right) + \left(\sum_{k=1}^{N} \rho Y_k V_k c_{pk}\right)\frac{\partial T}{\partial z} + \sum_{k=1}^{N}(h_k W_k \omega_k) = 0 \tag{7}$$

The equation of state for a mixture of perfect gases takes the form: $\rho = p/r_g T$, where $r_g = R/W$ and W is the molar mass such that: $1/W = \sum_{k=1}^{N}(Y_k/W_k)$.

In these equations, the mass density, ρ, the temperature, T, and species mass fractions Y_k, are functions of the spatial variable z. $U(z)$ defines the profile of u with respect to z, μ and λ respectively designate the local mixture viscosity and conductivity. V_k is the diffusion velocity of the k^{th} species, W_k is the molar mass of the k^{th} species and ω_k represents its molar rate of production. c_p denotes the local constant pressure heat capacity of the mixture and c_{pk} is the constant pressure heat capacity of the k^{th} species. h_k is the specific enthalpy.

The diffusion velocity V_k is computed from:

$$V_k = -\frac{D_k}{X_k}\frac{\partial X_k}{\partial z} + V_c \tag{8}$$

where D_k is the diffusion coefficient of the k^{th} species in the mixture, X_k is the mole fraction and V_c is a correction velocity given by:

$$V_c = \sum_{j=1}^{N} Y_j \frac{D_j}{X_j}\frac{\partial X_j}{\partial z} \tag{9}$$

The radiation heat loss from the flame zone is neglected. This may be significant at low strain rates but it is negligible in the range of strain rates considered in this article. Only the subcritical case is examined. This is acceptable if the extinction conditions determined at low pressure are a lower bound for the values at high pressures. This property is found in the experimental results of [11] and is also confirmed later for hydrogen/liquid oxygen flames. Only the gaseous phase is simulated, assuming that the liquid phase is pure oxygen. It is convenient to choose a pressure of 1 bar (0.1 MPa) initially, since reaction schemes and transport data are well validated. The process is then repeated at 2 bar in order to confirm the trend with increasing pressure. The calculations at higher subcritical pressures will require that the pressure- dependence of rate constants be taken into account. At supercritical pressures it would be necessary to modify the boundary value problem and consider the oxygen and hydrogen streams simultaneously.

The numerical technique is similar to that employed in reference [15]. Transport properties are obtained from the 'Transport' package [16]. Complex chemistry and thermodynamic properties are handled with 'Chemkin' software [17]. The corresponding databases have been verified between 80 K and 3000 K. The reaction mechanism, taken from reference [18] has 9 species and 14 reactions. For convenience the ideal gas equation of state is used, since it is very close to the Soave-Redlich-Kwong (SRK) equation of state in the gaseous phase at 1 bar.

2.3. Boundary conditions

A strain rate ε_s is imposed on the hydrogen side, leading to the following boundary conditions at $z = +\infty$: $U = \varepsilon_s$, $T = T_{H2}$, $Y_k = 1$ for hydrogen, $Y_k = 0$ otherwise; $\partial v/\partial z = -\varepsilon_s$.

The boundary conditions at the oxygen surface are quite different. Assuming that the liquid oxygen is at rest, the no-slip condition is expressed as:

$$U = 0 \tag{10}$$

Oxygen is the only species which can cross the surface. Its mass fraction is deduced from the Clausius-Clapeyron equation (Eq. 1):

$$Y_{1s} = \frac{W_1}{W}X_{1s} = \frac{W_1}{W}\frac{p_0}{p}\exp\left\{\frac{\Delta h_v}{r_g}\left[\frac{1}{T_0} - \frac{1}{T_s}\right]\right) \tag{11}$$

where $X_1 = p_s/p$ is the mole fraction of gaseous oxygen in the vicinity of the liquid surface. Close to the surface, oxygen is the main species in the mixture and it is possible to take $W \approx W_1$ and estimate r_g by R/W_1. The heat balance at the surface is given by expression (2).

The remaining constraints are expressed in terms of the diffusion velocities V_k. The mass flux of oxy-

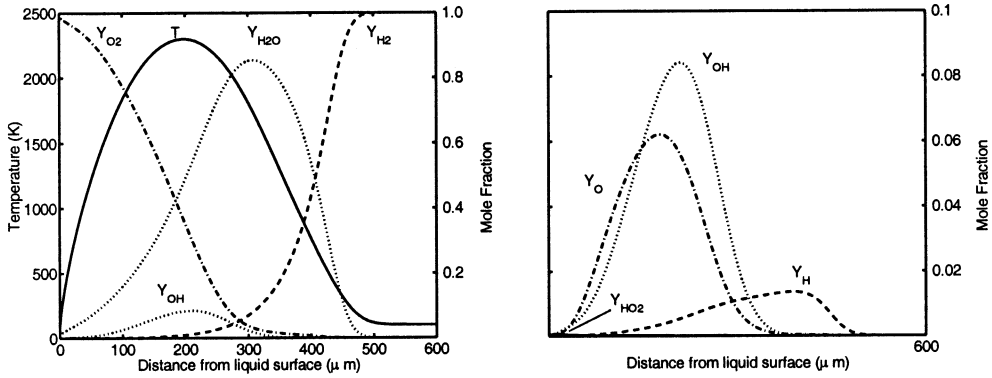

Fig. 4. Temperature and mole fraction profiles for a counterflow hydrogen flame above a condensed oxygen surface. Temperature and major species are plotted on the left, minor species on the right. The inlet hydrogen temperature is 100 K and the strain rate is 6×10^4 s^{-1} on the hydrogen side.

gen across the surface must equal the bulk mass flux away from the surface:

$$(\rho Y_{1s})v_{net1} = \rho v \tag{12}$$

where $v_{net1} \equiv (v + V_1)$ is the net velocity of species 1. This leads to:

$$V_1 = v\,(1 - Y_{1s})/Y_{1s} \tag{13}$$

As would be expected, the oxygen diffusion velocity V_1 tends to zero as Y_{1s} tends to 1. The net velocities of the remaining species must be zero. Hence:

$$V_k = -v \text{ for } k = 2,N \tag{14}$$

The system of equations is discretized using a centered finite difference scheme. Integration is achieved by combining a time-stepping scheme with Newton iterations on an adaptive mesh [15].

3. Results

In rocket engines, oxygen is injected at ~80 K. The liquid surface temperature is ~90 K. The first set of simulations assumes that the amount of energy used to heat up the liquid oxygen is negligible compared with the amount required to transform it from liquid to gas. Consequently the second term on the right hand side of Eq. 2 is set to zero. This assumption is later shown to be acceptable.

3.1. Species profiles in the flame

Typical profiles of temperature and mole fractions of species are shown in Fig. 4. For comparison the same profiles are displayed in Fig. 5 for a gaseous H_2/gaseous O_2 flame [19]. In both cases the hydrogen temperature is 100K and the strain rate on the hydrogen side is $\epsilon_s = 6.0 \times 10^4$ s^{-1}. The major species profiles are similar and the flames are about the same width. The temperature profile differs on the oxygen side in order to ensure that a temperature gradient exists at the liquid surface. The maximum temperature is also consistently higher, which reflects a higher residence time in the flame front. It is interesting to note that, in both cases, the temperature profile does not coincide with the H_2O profile, an effect which is associated with the decomposition of H_2O to OH at high temperature. This can be compared with the experimental results of [12] for a heptane/air flame. All major features are qualitatively identical but, for the hydrocarbon/air flame, the CO_2

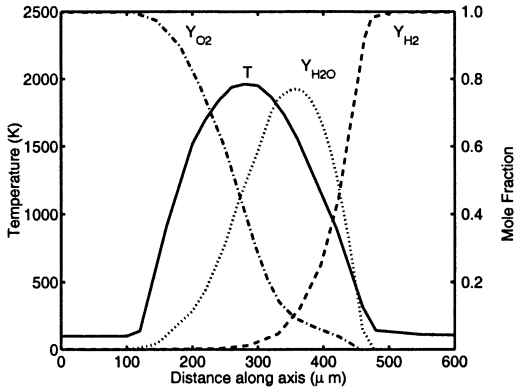

Fig. 5. Temperature and mole fraction profiles for a counterflow gaseous hydrogen/gaseous oxygen flame calculated by Schreiber (19). Both gases are injected at 100 K. The strain rate is 6×10^4 s^{-1}. The axis position is arbitrarily defined.

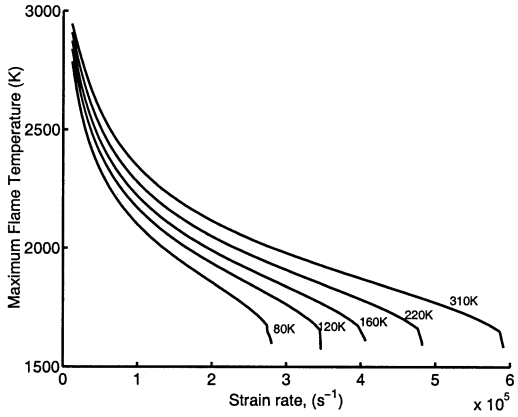

Fig. 6. Maximum flame temperature as a function of strain rate for a counterflow hydrogen flame above a condensed oxygen surface. The inlet hydrogen temperatures are shown next to each curve.

and H_2O profiles are nearly coincident with the temperature profile.

The flame thickness, δ_f, is defined as the distance between the points where the temperature is 5% of its minimum value. The flame is ~400 μm thick and its location, defined here by the position of the maximum flame temperature, is at $L_c = 200$ μm from the liquid surface. This latter value is an order of magnitude larger than that found in reference [9] and this does not change when a faster chemistry is employed, leading to a thinner flame. The position of a diffusion flame is determined to a great extent by the transport properties of the reactant streams and this may explain the difference between results obtained with a detailed model and estimates from a simplified analysis relying on a constant Lewis number approximation [9].

The oxygen mass fraction in the vicinity of the surface is 0.986. This reinforces the assumption that, in the neighbourhood of the interface, the amount of gas mixed with oxygen is negligible. The remaining fraction of 0.014 is almost entirely comprised of H_2O and a more rigorous analysis could consider this binary mixture at the interface.

3.2. Effect of strain rate

The maximum flame temperature is plotted as a function of strain rate, ϵ_s, in Fig. 6. It is shown for five values of the inlet hydrogen temperature between 80 K and 310 K. The maximum flame temperature decreases as strain increases since the increased gradients in the flame lead to a higher heat flux away from the flame. When the flame temperature is reduced below 1600 K, chain-breaking reactions overtake chain-branching steps and the flame is extinguished.

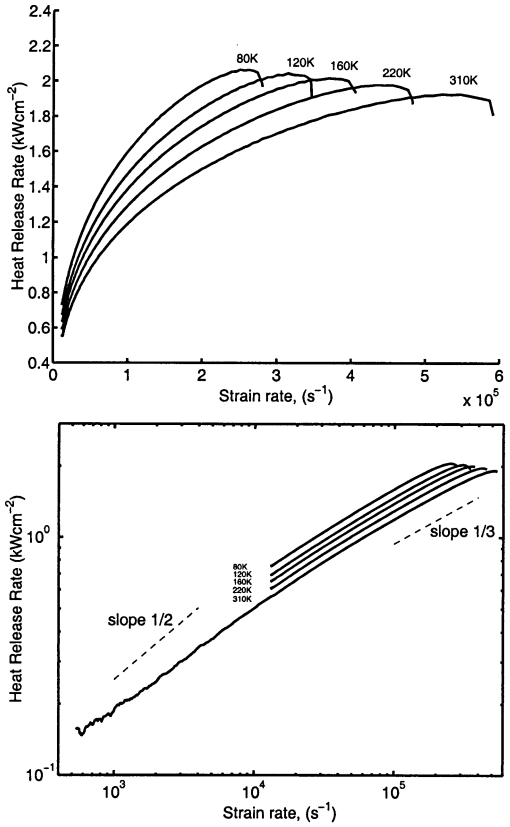

Fig. 7. Heat release rate per unit surface as a function of strain rate for a counterflow hydrogen flame above a condensed oxygen surface. The inlet hydrogen temperatures are shown next to each curve. At low strain rates, the heat release rate increases as $\epsilon_s^{1/2}$ in line with calculations in the infinitely-fast chemistry limit. When the flame thickness is of the same order as the flame stand-off distance, the slope becomes nearer to $\epsilon_s^{1/3}$.

The heat release rate per unit area ($\dot{q}_s = -\int \Sigma_{k=1}^{N} h_k W_k \omega_k dz$) is shown in Fig. 7 as a function of strain rate. In steady state, the heat release rate is proportional to the oxygen evaporation rate. The heat release rate varies with $\epsilon_s^{1/2}$ in the gas/gas counterflow situation according to the infinitely fast chemistry theory. The same dependence is obtained for the flame above a liquid fuel in the infinitely fast chemistry limit [9]. It is interesting to see if this result holds in the finite chemistry case. The numerical simulations presented here are interesting, since they show that the heat release rate evolves from a $\epsilon_s^{1/2}$ dependence at low strain rates, where the flame is far from the surface to a $\epsilon_s^{1/3}$ dependence at high strain rates, where the flame is close to the surface. When

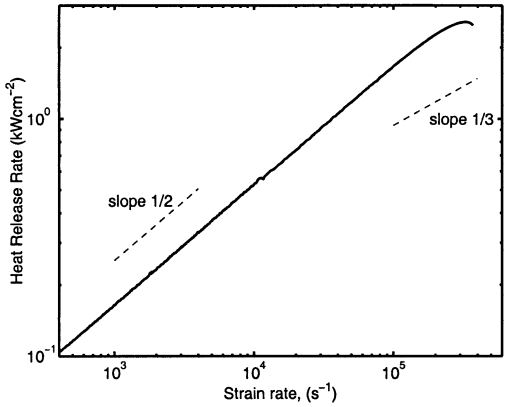

Fig. 8. Heat release rate as a function of strain rate for a flame above a liquid surface. Complex chemistry is replaced with a single step reaction and the parameters are chosen to give a thin flame with a similar value of heat release. The heat release rate increases as $\epsilon_s^{1/2}$ in line with calculations in the infinitely-fast chemistry limit.

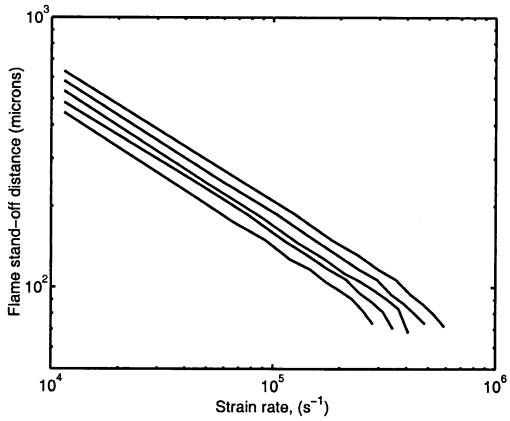

Fig. 9. Flame stand-off distance as a function of strain rate for a hydrogen flame above a condensed oxygen surface. It is proportional to $\epsilon_s^{-1/2}$, in line with predictions in the infinitely fast chemistry limit. The hydrogen temperatures are, from the top to the bottom curves: 310, 220, 160, 120, and 80 K.

the reaction expression is altered to make the flame thinner, as in figure 8, the dependence on $\epsilon_s^{1/2}$ is retained over a wider range of strain rates. Thus, it appears that, when the ratio of flame stand-off distance to flame thickness L_c/δ_f is small, the classical relationship between reaction rate and strain rate is altered by effects of vaporization at the liquid/gas interface.

The numerical values of the heat release rate found here are close to those obtained for a purely gaseous oxygen/hydrogen diffusion flame [19]. The heat release increases with strain rate up to the point of extinction because the species and temperature gradients become steeper, leading to faster mass diffusion to the flame. As the inlet hydrogen temperature decreases, the heat release per unit area increases. This is due to the higher density, which is a consequence of the lower flame temperature at a given strain rate.

The flame stand-off distance (defined as the distance from the oxygen surface to the point of maximum temperature) is shown as a function of strain rate in Fig. 9. This distance is proportional to $\epsilon_s^{-1/2}$, which agrees with the results in reference [9].

3.3. Effect of inlet hydrogen temperature on extinction strain rate

The extinction strain rate plotted as a function of inlet hydrogen temperature is shown in Fig. 10. The solid line represents conditions under which the thermodynamic and transport data have been verified for all species. The dotted line represents the results at lower inlet hydrogen temperatures. The correlations for the thermodynamic and transport data have been checked in this temperature range only for pure hydrogen. At the outer edge of the convection/diffusion zone other species are present below 80 K in very small concentrations. The transport correlations for these species are reasonable in this range and, although they are not strictly valid, the error is likely to be minimal.

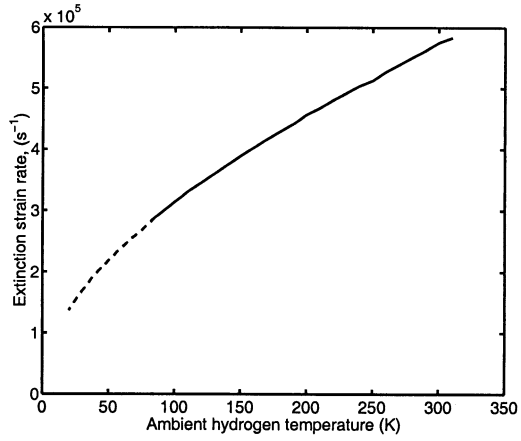

Fig. 10. Extinction strain rate plotted as a function of inlet hydrogen temperature. The solid line represents the region in which thermodynamic and transport properties of all species have been verified. The dotted line represents the region in which only hydrogen properties have been verified.

In any case, it is apparent that the extinction strain rates are in excess of $10^5\ s^{-1}$. These values are much larger than the strain rates which may be expected in the jet flames formed by coaxial injectors in typical rocket motors. A rough estimate of the maximum aerodynamic strain rate may be obtained, for example, by considering a hydrogen eddy at 100 ms^{-1} impinging perpendicularly onto the oxygen surface and decelerating to a stagnation value within $l \approx 1$ mm. This would yield a strain rate of $\epsilon_s \approx 10^5\ s^{-1}$, which would still not be sufficient to extinguish the flame. Real conditions are less severe than this. The scale l is estimated by assuming that it is of the order of a typical dimension of the injector. The LOx tube diameter is a few mm and the hydrogen annulus is of the order of a mm. Another possibility would be to estimate the scalar dissipation in the hydrogen jet, which could then be compared with the critical scalar dissipation inducing extinction.

3.4. Effect of a temperature gradient in the liquid oxygen

Heat conduction into the liquid oxygen core only affects the flame when it is of the same order of magnitude or greater than the vaporization heat flux. The simulations show that the latter is greater than $10^5\ Wm^{-2}$ for strain rates above $10^4\ s^{-1}$. Given that the thermal conductivity of liquid oxygen is $\lambda = 0.16\ Wm^{-1}K^{-1}$, a temperature gradient of at least $10^6\ Km^{-1}$ is required for the flame to be affected. The oxygen's surface temperature is ~10 K higher than its core temperature. A thermal boundary layer will exist between the surface and the core. For ease of demonstration, one can assume a linear temperature profile. For the flame to be affected, this layer must be less than 10 μm thick. This is confirmed in Fig. 11. where the maximum flame temperature is shown as a function of thermal boundary layer thickness at a strain rate of $1.4 \times 10^4 s^{-1}$. The flame is only affected when the layer is <10 μm thick and extinguishes when it is 0.5 μm thick. A thermal layer this thin will not last for any appreciable distance beyond the injection plane. Consequently, it is reasonable to neglect heat conduction into the liquid oxygen.

3.5. Effect of pressure

The effect of pressure on strained laminar diffusion flames is studied via an asymptotic analysis in appendix A, assuming infinitely fast chemistry, equal diffusivities, $\rho^2 D$ independent of temperature and $D \propto p^{-1}$. The analysis indicates that the heat release per unit surface is proportional to $(\epsilon_s p)^{1/2}$. The fact that the heat release rate increases with pressure while the thermal conductivity remains approximately constant

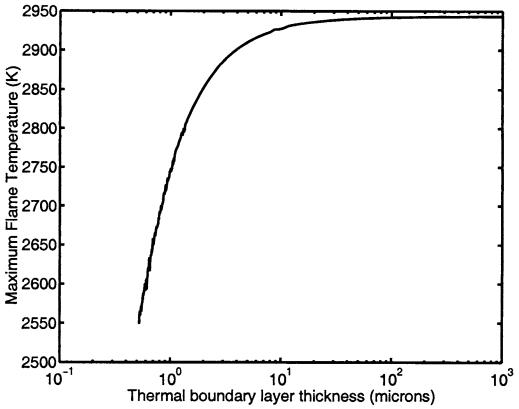

Fig. 11. Maximum flame temperature as a function of thermal boundary layer thickness at the condensed oxygen surface. The temperature drop across the layer is 10 K and the profile is assumed to be linear. The strain rate is $1.4 \times 10^4 s^{-1}$. It can be seen that the thermal layer needs to be unrealistically thin before it can have an effect on the flame.

suggests that the extinction strain rate will also increase with pressure. This is consistent with experimental results [11] which show that the extinction strain rate increases asymptotically to a maximum between 3 and 10 bar for a heptane/air flame.

The 1-D simulations were repeated at 2 bar to check this tendency. The flame is thinner and is slightly closer to the condensed surface at a given strain rate. Figure 12 shows the heat release rate as a function of strain rate. In accordance with the asymp-

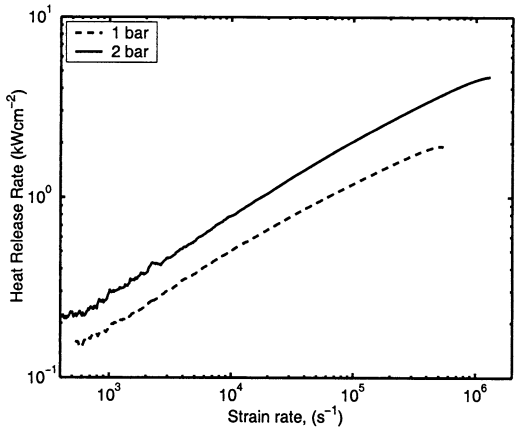

Fig. 12. Heat release rate per unit area as a function of strain rate for a hydrogen flame above a condensed oxygen surface at 1 bar and 2 bar pressure. The inlet hydrogen temperature is 310 K. The extinction strain rate increases by a factor of 2.

totic analysis, the heat release increases (although in proportion to $\epsilon_s^{1/2} p^{4/5}$) and the flame withstands higher strain rates before extinction. It is not possible to predict how the pressure dependence law will evolve as pressure is increased but this aspect deserves further consideration.

4. Conclusions

Flame stabilization is critical for the successful operation of rocket motors, which often use liquid oxygen and gaseous hydrogen. The flame lies close to the LOx surface and a possible extinction mechanism is via excessive strain against the cold liquid surface. The most severe scenario arises when an eddy impinges perpendicularly to the surface. This corresponds to a counterflow diffusion flame above a liquid reactant and constitutes a model problem in combustion science.

A counterflow diffusion flame between a hydrogen stream and a surface of condensed oxygen has been studied at pressures of 1 and 2 bar using a one-dimensional numerical formulation. Species profiles are similar to those found in gaseous diffusion flames. The temperature profile is also similar but it features a gradient at the surface, which is required to evaporate the oxygen. The flame structures are also in qualitative agreement with results in the infinitely-fast chemistry limit [9] where the extinction limit strain rate cannot be determined. The present calculations provide numerical values for the rate of heat release per unit flame surface, the flame stand-off distance, the extinction strain rates and extinction temperatures.

The extinction strain rate decreases as the ambient hydrogen temperature decreases but it remains extremely high. It is an order of magnitude greater than the highest strain rates found in jet flames formed by typical rocket motor injectors. This means that if a flame edge exists in the wake of the oxygen injector lip, the subsequent diffusion flame cannot be extinguished downstream. This reduces the question of flame stabilization to a study of the zone behind the lip, which can be approached via numerical calculations [4].

Heat conduction into the liquid oxygen is negligible compared with the heat flux required to vaporize it. This suggests that the temperature of the oxygen jet is not a critical factor.

Around and above the critical pressure of oxygen, the oxygen surface boundary condition of this one-dimensional model is no longer valid. In this case a rapidly changing density layer is found between the hydrogen and oxygen streams. This must be resolved by a well-chosen equation of state. However, this study implies that the extinction strain rate increases with pressure. Since conditions at the surface seem relatively unimportant, it is a fair assumption that the extinction strain rate is even higher at supercritical pressures than at subcritical pressures.

Acknowledgments

This work has been partially supported by CNES and SNECMA in the framework of the GDR “Combustion in Liquid Rocket Engines”.

References

[1] J. Oefelein, V. Yang, J. Propul, Power 14 (5) (1998) 843–857.
[2] W. Mayer, H. Tamura, J. Propul, Power 12 (6) (1996) 1137–1147.
[3] G. Herding, R. Snyder, P. Scouflaire, C. Rolon, S. Candel, Twenty-Sixth Symposium (International) on Combustion, 1996 The Combustion Institute, Pittsburgh, p. 2041.
[4] M. Juniper, Structure et stabilisation des flammes cryotechniques, Ph.D. thesis, Ecole Centrale de Paris, Chatenay-Malabry, France (2001).
[5] D. Preclik, P. Spagna, Low frequency and high frequency combustion oscillation phenomena inside a rocket combustion chamber fed by liquid or gaseous propellants, AGARD Conference Proceedings, Vol. 450, 1988, p. 6–1.
[6] J. Lee, C. Frouzakis, K. Boulouchos, Proc. Combus. Instit. 28 (2000) 801–806.
[7] F. Fendell, J. Fluid Mech. 21 (1965) 281–303.
[8] A. Hamins, K. Seshadri, Twentieth Symposium (International) on Combustion, 1984, The Combustion Institute, Pittsburgh, p. 1905.
[9] A. Burluka, R. Borghi, Combust. Flame 122 (2000) 227–232.
[10] V. Katta, W. Roquemore, Proc. Combust. Instit. 28 (2000) 2055–2062.
[11] T. Niioka, S. Hasegawa, T. Tsukamoto, J. Sato, Combus. Flame 86 (1991) 171–178.
[12] J. Kent, A. Williams, Fifteenth Symposdium (International) on Combustion, 1975, The Combustion Institute, Pittsburgh, p. 315.
[13] J. Daou, P. Haldenwang, C. Nicoli, Combust. Flame 101 (1995) 153–169.
[14] D. Schlotz, E. Gutheil, Combust. Sci. Technol. 158 (2000) 195–210.
[15] N. Darabiha, Combust. Sci. Technol. 86 (1992) 163–181.
[16] R. Kee, G. Dixon-Lewis, J. Warnatz, M. Coltrin, J. Miller, A Fortran computer code package for the evaluation of gas phase multicomponent transport properties, Tech. Rep. SAND86-8246 UC-401, Sandia National Laboratories (1986).
[17] R. Kee, F. Rupley, J. Miller, A fortran chemical kinetics package for the analysis of gas phase chemical

kinetics, Tech. Rep. SAND89-8009B UC-706, Sandia National Laboratories (1989).
[18] P. Lindstedt, Twenty-Seventh Symposium (International) on Combustion, 1998, The Combustion Institute, Pittsburgh, p. 269.
[19] D. Schreiber, Quelques problèmes de combustion liés à l'allumage dans les moteurs fusée cryotechniques, Ph.D. thesis, Ecole Centrale de Paris, Châtenay-Malabry, France (1991).

Appendix A. Consumption rates in strained laminar diffusion flames

A counterflow diffusion flame is considered between two reactants, labelled 1 and 2. Let G_α and D_α represent the consumption rate and diffusivity of reactant α [15]. The mass stoichiometric ratio s characterizes the single step chemical reaction $F + sO \rightarrow P$. An asymptotic analysis at constant strain rate, ϵ_s, in the limit of infinitely fast chemistry and with $\rho^2 D$ independent of temperature gives:

$$G_\alpha = \rho Y_{\alpha 0}\left(\frac{2D_{\alpha 0}\epsilon_s}{\pi}\right)^{1/2}\frac{\exp^{-\eta_{\alpha f}^2}}{1-\mathrm{erf}(\eta_{\alpha f})} \tag{A.1}$$

where η is a transformed spatial coordinate and the subscript f denotes the flame position. The flame positions $\eta_{\alpha f}$ are solutions of the trancendental equation:

$$e^{-\eta_{1f}^2(\beta^2-1)}\frac{1-\mathrm{erf}(\eta_{1f})}{1+\mathrm{erf}(\eta_{1f}\beta)} = \beta\phi \tag{A.2}$$

where the global mixture ratio, ϕ, compares conditions prevailing at infinity to the mass stoichiometric ratio:

$$\phi = sY_{10}/Y_{20} \tag{A.3}$$

β designates the square root of the diffasivity ratio: $\beta = (D_{10}/D_{20})^{1/2}$, which means one can write $\eta_{2f} = \beta\eta_{1f}$. If $\beta = 1$ then the consumption rates are given by:

$$G_1 = \rho Y_{10}\frac{1+\phi}{\phi}\left(\frac{D\varepsilon_s}{2\pi}\right)^{1/2} e^{-\eta_f^2} \tag{A.4}$$

$$G_2 = \rho Y_{20}(1+\phi)\left(\frac{D\varepsilon_s}{2\pi}\right)^{1/2} e^{-\eta_f^2} \tag{A.5}$$

with η_f defined implicitly by $\mathrm{erf}(\eta_f) = (1-\phi)/(1+\phi)$. (A crude approximation of the error function when $\eta_f \approx 0$ is simply $\mathrm{erf}(\eta_f) \sim 2\eta_f/\sqrt{\pi}$). It is now necessary to evaluate $\rho^2 D$ as a function of pressure:

$$\rho^2 D(p,T) = \rho^2(p,T)\,D(p,T)$$

However, $\rho^2 D$ is supposed independent of temperature and can be evaluated at a reference temperature. Keeping the pressure constant one may write:

$$\rho^2 D(p,T) = \rho^2(p,T_{ref})\,D(p,T_{ref})$$

Now D is inversely proportional to pressure:

$$D(p,T_{ref}) = \frac{p_{ref}}{p}D(p_{ref},T_{ref})$$

Thus

$$\rho^2 D(p,T) = \rho^2(p,T_{ref})\frac{p_{ref}}{p}\,D(p_{ref},T_{ref})$$

or

$$\rho^2 D(p,T) = \left(\frac{p}{rT_{ref}}\right)^2\frac{p_{ref}}{p}\,D(p_{ref},T_{ref})$$

$$= \left(\frac{p_{ref}}{rT_{ref}}\right)^2\frac{p}{p_{ref}}\,D(p_{ref},T_{ref})$$

One may also write:

$$\rho^2 D = \frac{p}{p_{ref}}\,[\rho^2 D]_{ref}$$

The final result is:

$$G = \rho_{ref}Y_{20}(1+\phi)\left(\frac{D_{ref}\epsilon_s}{2\pi}\right)^{1/2}\left(\frac{p}{p_{ref}}\right)^{1/2}\exp(-\eta_f^2) \tag{A.6}$$

from which it can be seen that the consumption rate and the heat release rate are proportional to the product $(\epsilon_s p)^{1/2}$. This indicates that the consumption rate per unit flame surface increases with the square root of the pressure.